Harmonic Suppressed Dual-Band Bandpass Filters With Tunable Passbands

Girdhari Chaudhary, *Student Member, IEEE*, Yongchae Jeong, *Senior Member, IEEE*, and Jongsik Lim, *Senior Member, IEEE*

***Abstract*—This paper presents a novel approach to the design of tunable dual-band bandpass filter with broadband harmonic suppression characteristics. The proposed filter structure offers the possibility of two tunable passbands, as well as a fixed first passband and controllable second passband. The tunable passband frequency usually causes a shift of the harmonics, which need to be suppressed to improve out-of the passband characteristics. In order to suppress the harmonics over a broad bandwidth, defected ground structures are used at input and output feeding lines without degrading the passbands characteristics. Both theory and experiment are provided to validate the proposed filter. From the experimental results, it is found that the proposed filter exhibits a first passband center frequency tunable range of 34.14% from 0.85 to 1.2 GHz with the almost constant 3-dB fractional bandwidth (FBW) of 13% and second passband center frequency tunable range of 41.81% from 1.40 to 2.14 GHz with the 3-dB FBW of 11%. The measured results of the proposed filters show a rejection level of 20 dB up to more than ten times of second passband frequency can be obtained, thereby ensuring broad harmonics rejection characteristics without degradation of passbands. The measurement data have good agreement with the simulation.**

***Index Terms*—Defected ground structure (DGS), dual band, harmonics suppression, tunable bandpass filter (BPF), varactor diode.**

I. Introduction

ELECTRICALLY tunable multiband microwave bandpass filters (BPFs) are essential components for the multiband wireless communication and radar systems due to their potential to significantly reduce system size and complexity. In order to meet these requirements, various approaches have been applied to design tunable BPFs using different kinds of tuning devices.

Today, microelectromechanical system (MEMS) devices are widely used to design tunable filters due to their high Q and high linearity [1]–[4]. However, the high cost and maturity of RF-MEMS technology limits their application in design of tunable devices. The tunable and reconfigurable BPFs can also be implemented using ferroelectric devices [5], [6], piezoelectric transducer [7], and p-i-n diodes [8].

Manuscript received December 19, 2011; revised March 22, 2012; accepted March 25, 2012. Date of publication May 24, 2012; date of current version June 26, 2012.

G. Chaudhary and Y. Jeong are with the Department of Electronics and Information Engineering, Information Technology Convergence Research Center, Chonbuk National University, Jollabuk-do 561-756, Korea (email: ycjeong@jbnu.ac.kr).

J. Lim is with the Department of Electrical and Communication Engineering, Soonchunhyang University, Chungcheongnam-do 336-745, Korea.

Color versions of one or more of the figures in this paper are available online at http://ieeexplore.ieee.org.

Digital Object Identifier 10.1109/TMTT.2012.2197020

Semiconductor varactors are also widely used in designing tunable BPFs due to high tuning speed and reliability. Hunter and Rhodes [9] and Kim and Yun [10] demonstrated a varactor tuned combline filter. Brown and Rebeiz [11] reported a four-pole varactor tuned interdigital filter. Park and Rebeiz [12] demonstrated two-pole tunable filters with the predefined bandwidth characteristics. Tang and Hong [13] designed the tunable BPF using dual-mode resonators. In order to improve the selectivity of BPFs, the filter with transmission zeros was presented in [14] and [15]. In [16], ferroelectric capacitors were used to design tunable BPFs for Ka- and U-band applications. In [17], a substrate integrated cavity filter with wide tuning range is presented. However, none of the above work addressed the design of two tunable passbands.

There have been some attempts to design the tunable dual-passband filters [18]–[21]. However, these works focused on the design of fixed first passband and controllable second passband. None of the above referenced works focused on design of two tunable passbands. Djoumessi *et al.* [22] demonstrated the varactor-tuned quarter-wavelength dual-band BPF, which had a huge circuit size, large number of varactor diodes, and biasing circuits.

With tunable passband frequency characteristic in the tunable filters, the harmonic bands, which degrade the out-of passband characteristics, are also tuned. Thus, the suppression of harmonics is one of the critical issues for the tunable filters. This issue has rarely been addressed in the design of tunable dual-band filters. However, some attempts have been made to solve this problem in the single-band tunable filters [23]–[25].

There have been few dual-band filters having fixed passbands incorporated with extension of the upper stopband rejection characteristics [26]–[28]. In [26], the distances among the higher order resonances of the hairpin resonators are limited so that the stopband performances need improving. The end-coupled stepped impedance resonators are used in [27] to achieve excellent stopband rejection. In [28], multiple transmission zeros are incorporated in order to obtain broadband harmonic suppression.

In this paper, tunable dual-band BPFs with broad harmonic suppressed characteristics are presented. From theoretical even- and odd-mode analysis, it is found that the first passband depends on an odd-mode capacitance, while the second passband depends on the even- and odd-mode capacitances. Therefore, the proposed filter structure offers the controllable two passbands, as well as a fixed first passband and controllable second passband.

To suppress the harmonics, a defected ground structure (DGS) is used at input/output feeding lines. The band-rejec-

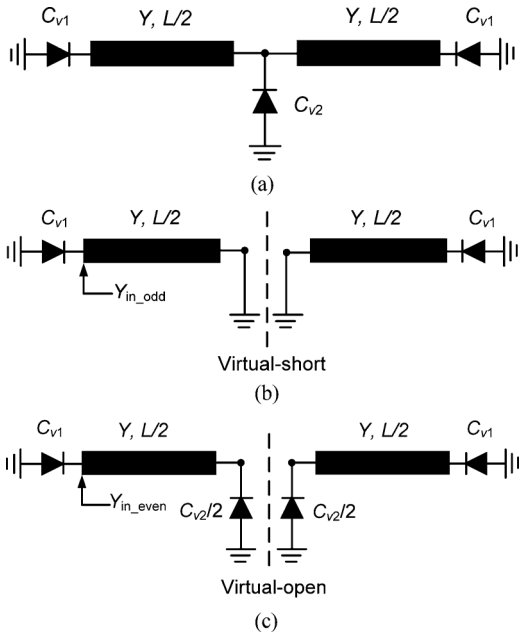

Fig. 1. (a) Basic structure of the proposed resonator. (b) Odd-mode excitation equivalent circuit. (c) Even-mode excitation equivalent circuit.

tion characteristics of the DGS are utilized to suppress the harmonics.

This paper is organized as follows. Firstly, the characteristics of proposed tunable resonators are discussed in Section II. Secondly, the design and implementation of the filters along with the simulation and measurement results are described in Section III, followed by a conclusion in Section IV.

II. Characteristics of Proposed Resonator

Fig. 1(a) shows the basic structure of the proposed resonator. It consists of a transmission line and three varactor diodes. For the theoretical analysis, it is assumed to be a lossless transmission line of characteristic admittance Y and physical length L. Two varactor diodes are attached at the ends of the transmission line and one varactor diode is placed at a center point of the transmission line. For simplicity, the parasitic elements of varactor diodes are ignored. Since the structure is symmetrical, the even- and odd-mode analysis method is applicable to obtain the resonant frequencies [25].

A. Odd-Mode Excitation Analysis

When the odd-mode excitation is applied to the ends of the proposed resonator shown in Fig. 1(a), there is a voltage null along the symmetry plane. Under the odd-mode excitation, it can be represented by the half circuit, as given in Fig. 1(b). The odd-mode input admittance is given as follows:

$$Y_{\text{in\_odd}} = j\left[\omega_{\text{odd}} C_{v1} - Y\cot\left(\frac{\beta L}{2}\right)\right] \tag{1}$$

where C_{v1} is the capacitance of the varactor diode connected at the end of the line and β is the propagation constant of the transmission line. From the resonance condition of $\text{Im}(Y_{\text{in-odd}}) = 0$, the odd-mode resonant frequency can be determined as follows:

$$f_{\text{odd}} \times \tan\left(\frac{\pi f_{\text{odd}} L}{v_p}\right) = \frac{Y}{2\pi C_{v1}} \tag{2}$$

where v_p is the phase velocity. The fundamental odd-mode resonant frequency can be used as the first passband frequency. From (2), it is concluded that the odd-mode resonant frequency fully depends on the capacitance C_{v1} of the varactor diode connected at the ends of the transmission line. Therefore, the change of the bias voltage on both end varactor diodes will result in the change of passband frequencies, enabling the tunability of the first passband frequency. Moreover, the odd-mode resonant frequencies are not affected by the varactor diode connected at the center of the transmission line.

B. Even-Mode Excitation Analysis

For the even-mode excitation, there is no current flowing through the center of the transmission line. Under the even-mode condition, the proposed resonator can be represented by the equivalent half circuit shown in Fig. 1(c). The even-mode input admittance is given as follows:

$$Y_{\text{in\_even}} = j\left(\omega_{\text{even}} C_{v1} + Y\frac{\omega\frac{C_{v2}}{2} + Y\tan(\frac{\beta L}{2})}{Y - \omega\tan(\frac{\beta L}{2})\frac{C_{v2}}{2}}\right) \tag{3}$$

where C_{v2} is the capacitance of the varactor diode connected at the center of the transmission line. For the resonance condition, the even-mode resonant frequency can be determined as

$$\left(f_{\text{even}} - \frac{Y^2}{2\pi^2 f_{\text{even}} C_{v1} C_{v2}}\right)\tan\left(\frac{\pi f_{\text{even}} L}{v_p}\right) = \frac{Y\left(C_{v1} + \frac{C_{v2}}{2}\right)}{\pi C_{v1} C_{v2}}. \tag{4}$$

The fundamental even-mode resonant frequency can be utilized as the second passband frequency. From (4), it is observed that the even-mode resonant frequency depends on C_{v1} and C_{v2}. Thus, the change of the bias voltages applied to all of the varactor diodes will also result in the change of passband frequencies, enabling the tunability of the second passband frequency. Moreover, when C_{v1} is fixed, the even-mode resonant frequency can tune with the help of C_{v2} alone. This characteristic of the proposed resonator can be used to design a dual-band BPF with controllable second passband (even-mode resonant frequency) and fixed first passband (odd-mode resonant frequency).

To verify the above theoretical analysis, a full-wave electromagnetic (EM) simulation was carried out by using Ansoft's HFSS v11. Two microstrip lines with a characteristic impedance of 50 Ω are utilized to feed the proposed resonator using loose coupling to investigate its resonant behavior. The length of resonator is fixed at 40 mm.

Fig. 2(a) shows the simulated S_{21}-magnitude of weak coupling resonator circuit according to different capacitances of varactor diodes. As capacitances are varied, the odd- and even-

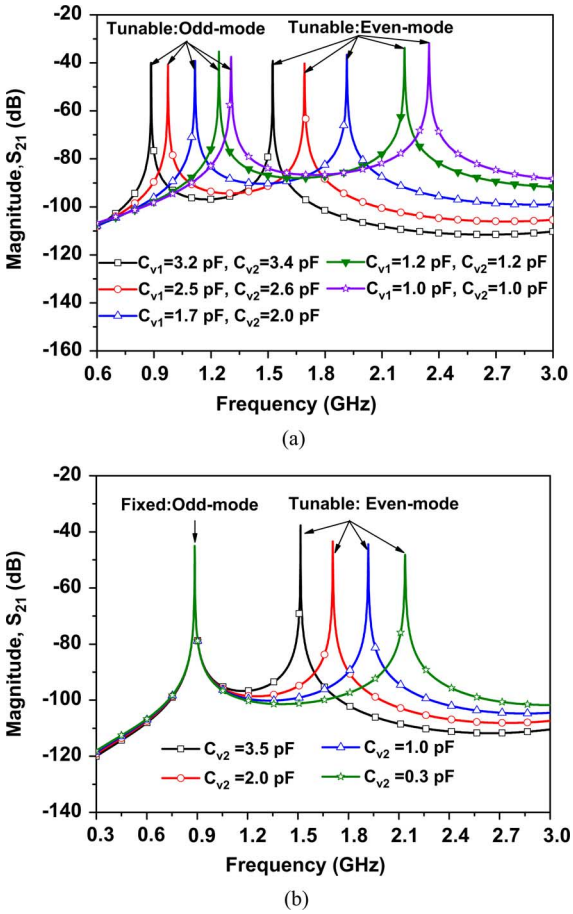

Fig. 2. Resonant frequencies according to capacitances. (a) Tunable odd and even mode. (b) Fixed odd-mode and tunable even-mode frequencies with fixed $C_{v1} = 3.2$ pF.

mode resonant frequencies are tuned simultaneously. This characteristic of the proposed resonator can be utilized to design a dual-band BPF with two controllable passbands.

Fig. 2(b) shows the simulated S_{21}-magnitude of the resonator circuit in the case where the capacitances of the varactor diodes connected at the end of the transmission line are fixed. Under this condition, it is obvious that the odd-mode resonant frequency is fixed and the even-mode resonant frequency can be tuned by varying the capacitance of the varactor diode connected at the center of the line. By varying the value of C_{v2} from 3.5 to 0.3 pF, the even-mode resonant frequency can be varied from 1.5 to 2.3 GHz. This characteristic of proposed resonator can be utilized to design a dual-band BPF with a fixed first passband and controllable second passband.

C. External Quality Factor (Q_e)

In order to find the external quality factor, the configuration of the tapped resonator is shown in Fig. 3. To facilitate the analysis, the effects of line discontinuity are ignored. The input admittance (Y_L) of the resonator seen from the center of the line is given as follows:

$$Y_L = j\left[\omega C_{v2} + Y\frac{\omega C_{v1} + Y\tan\left(\frac{\omega L}{v_p}\right)}{Y - \omega C_{v1}\tan\left(\frac{\omega L}{v_p}\right)}\right]. \quad (5)$$

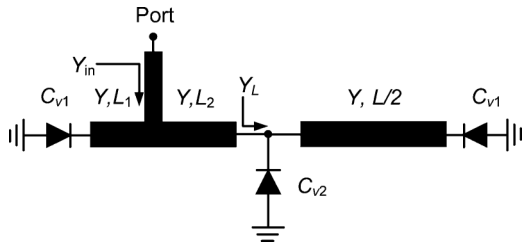

Fig. 3. Resonator with input coupling network.

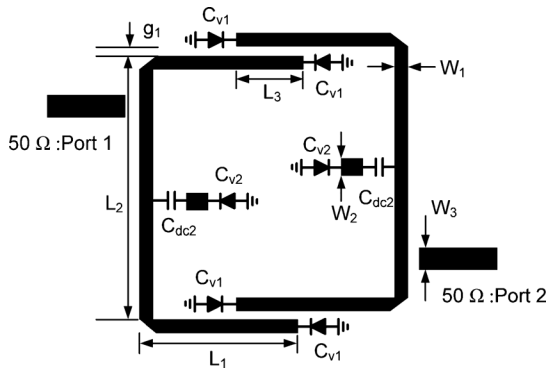

Fig. 4. Layout for examining the coupling between resonators: physical dimensions: $L_1 = 17.2$, $L_2 = 34.28$, $L_3 = 14$, $W_1 = 1.8$, $W_2 = 1.8$, $W_3 = 2.4$, $C_{dc1} = 20$ pF, and $C_{dc2} = 3.90$ pF. (Physical unit: millimeters).

The overall input admittance (Y_{in}) of resonator seen from the input port is given as follows:

$$Y_{in} = j\left[\frac{\omega C_{v1} + Y\tan\left(\frac{\omega L_1}{v_p}\right)}{Y - \omega C_{v1}\tan\left(\frac{\omega L_1}{v_p}\right)}\right] + Y\frac{Y_L + jY\tan\left(\frac{\omega L_2}{v_p}\right)}{Y + jY_L\tan\left(\frac{\omega L_2}{v_p}\right)}. \quad (6)$$

The external quality factor (Q_e) is then determined as follows [24]:

$$Q_e = \frac{\omega_0}{2Y_0}\frac{\partial \mathrm{Im}\left[Y_{in}\right]}{\partial\omega}\bigg|_{\omega=\omega_0}. \quad (7)$$

It can be seen that the lengths of the transmission line L_1 and L_2 will affect Q_e. By properly choosing these parameters, the desired Q_e can be obtained within the frequency tuning range.

D. Coupling Coefficient (K_i)

Fig. 4 shows the arrangement of resonators for EM simulation to analyze the coupling coefficient between resonators according to two parameters, g_1 and L_3, which are gap between the resonators and coupling length of two resonators, respectively. The other parameters used in the simulation are shown in Fig. 4. To decrease the effect of input/output line on the coupling coefficient between resonators, a weak input/output feed is used in this filter. In this simulation, the ideal capacitors were used. The coupling characteristic between resonators are simulated and drawn with respect to g_1 in Fig. 5. As seen from Fig. 5, the separation of resonant frequencies can be controlled with g_1.

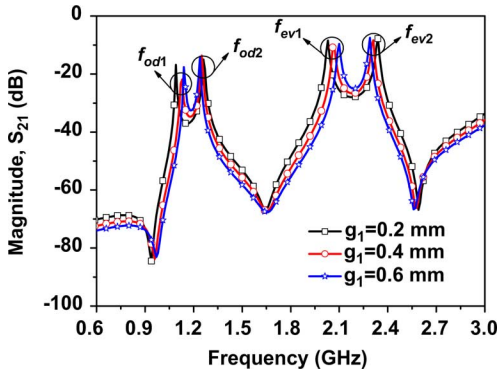

Fig. 5. Coupling characteristic between resonators with respect to g_1 in case of $L_3 = 10$ mm, $C_{v1} = 1$ pF, and $C_{v2} = 0.9$ pF.

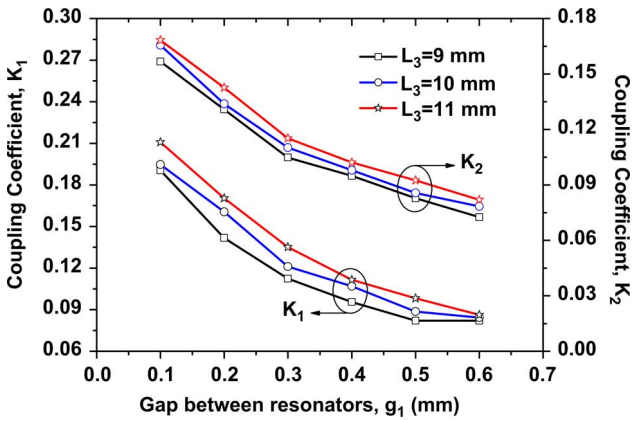

Fig. 6. Calculated coupling coefficient with respect to g_1 and L_3 in case of $C_{v1} = 1$ pF and $C_{v2} = 0.9$ pF.

For sake of estimating and designing the two passbands, the coupling amounts of two bands can be calculated by the following common formulas [29]:

$$K_1 \approx \frac{f_{\mathrm{od2}}^2 - f_{\mathrm{od1}}^2}{f_{\mathrm{od2}}^2 + f_{\mathrm{od1}}^2} \quad K_2 \approx \frac{f_{\mathrm{ev2}}^2 - f_{\mathrm{ev1}}^2}{f_{\mathrm{ev2}}^2 + f_{\mathrm{ev1}}^2} \tag{8a}$$

$$\frac{K_1}{K_2} \approx \frac{\Delta_1}{\Delta_2} \tag{8b}$$

where K_1 and K_2, $f_{\mathrm{od}i}$, $f_{\mathrm{ev}i} (i = 1, 2)$ are coupling-coefficient, odd- and even-mode resonant frequencies at first and second passbands, respectively. With combined adjustments of f_{od1}, f_{od2}, f_{ev1}, and f_{ev2}, the first and second passbands are established and determined. Therefore, bandwidth of the two passbands can be controlled by changing their coupling coefficients. For a design graph chart, the coupling behaviors between resonators are simulated and estimated coupling amounts are drawn in Fig. 6 as a function of g_1 and L_3.

III. Filter Implementation and Verification

To verify the analytical analysis of the proposed resonators, two types of tunable dual-band BPFs were designed, simulated, and measured. The used substrate is an RT/Duriod 5880 made by the Rogers Corporation with a dielectric constant (ε_r) of 2.2 and thickness (h) of 31 mil.

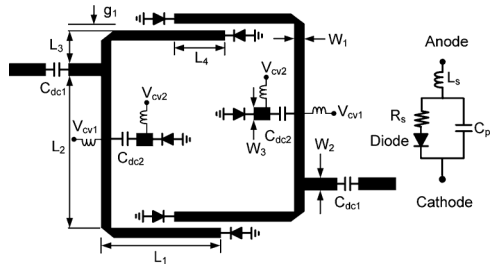

Fig. 7. Configuration of filter I with physical dimensions and varactor diode equivalent circuit model: $L_1 = 17.2$, $L_2 = 27.6$, $L_3 = 5.3$, $L_4 = 10$, $W_1 = 1.8, W_2 = 2.4, W_3 = 1.8, g_1 = 0.4, C_{\mathrm{dc1}} = 20$ pF, $C_{\mathrm{dc2}} = 3.90$ pF, $C_p = 0.51$ pF, $R_s = 1.2\ \Omega$, $L_s = 0.7$ nH. (Physical unit: millimeters).

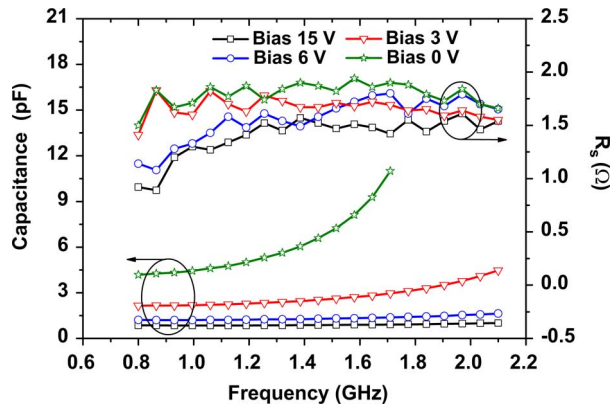

Fig. 8. Measured capacitance and series resistance (R_s) of the varactor diode SMV 1233-079LF.

A. Filter I: Tunable Dual-Band BPF Without Harmonic Suppression

Fig. 7 depicts the configuration of the second-order microstrip tunable dual-band filter I. In the proposed filter, four varactors are attached at the ends of the two microstrip lines and two varactor diodes are attached at the center of the two microstrip lines.

The resonators are folded in order to reduce the size, forming open loops. The varactor diodes are SMV1233–079LF from Skyworks Solutions Inc. The input/output lines are tapped at the resonators. Two capacitors (C_{dc1}) are attached in the feeding lines, functioning as a dc block. Another two dc block capacitors (C_{dc2}) are attached at the center of line.

The simulation was accomplished by using Agilent Technologies' 2011 Advanced Design System (ADS). In this simulation, the SPICE model of the varactor diode provided by the manufacturer was used, as shown in Fig. 7. After the simulation, the physical parameters and component values of the filter are determined as shown in Fig. 7. The measured capacitance and series resistance (R_s) of the varactor diode is shown in Fig. 8.

Fig. 9 shows the simulation and measurement results of filter I for several typical bias voltages. The measurement results agree well with the simulation results. The measurement results show that the first passband frequency can be tuned from 0.85 to 1.2 GHz with almost constant 3-dB FBW of 13% and the second

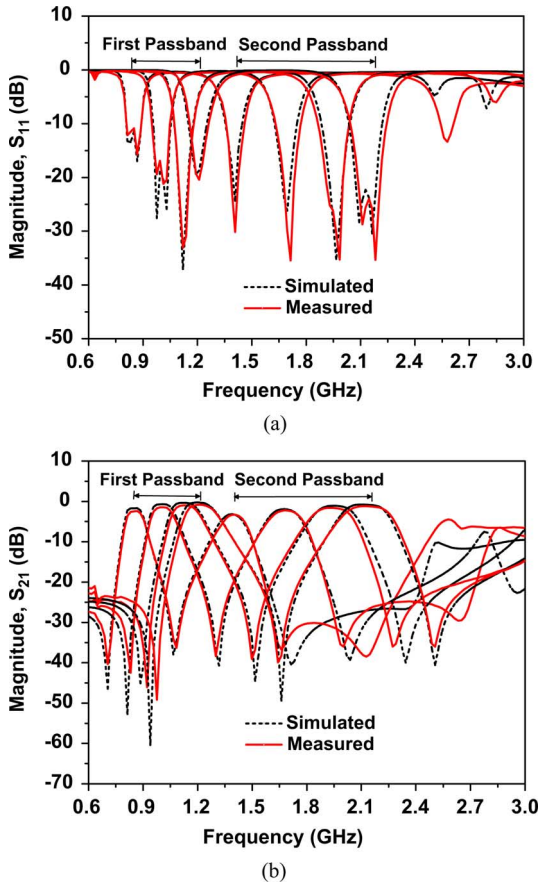

Fig. 9. Simulation and measurement results of filter I with tunable both passbands. (a) Return loss. (b) Insertion loss. Reverse bias voltage variation: $V_{Cv1} = 1.5 \sim 15$ V and $V_{Cv2} = 0.4 \sim 15$ V.

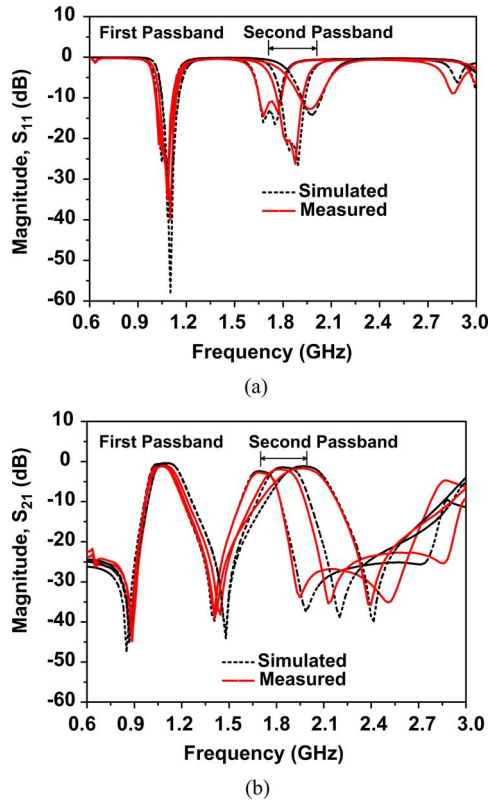

Fig. 10. Simulation and measurement results of filter I with fixed first passband and tunable second passband. (a) Return-loss and (b) insertion-loss characteristics. Reverse-bias voltage variation: $V_{Cv1} = 5.45$ V and $V_{Cv2} = 3.08 \sim 15$ V.

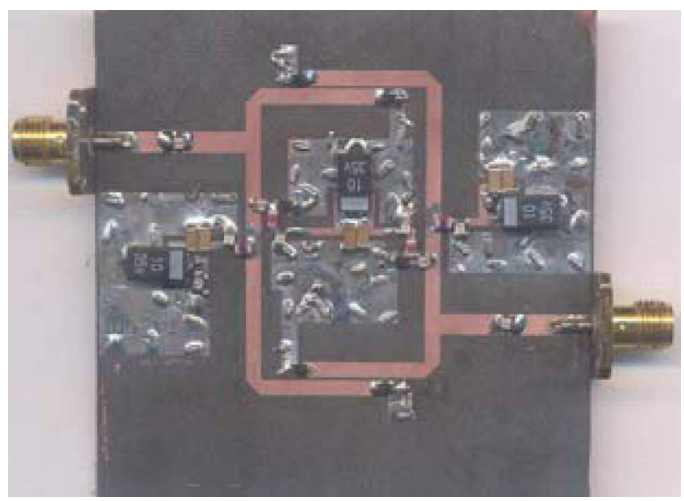

Fig. 11. Photograph of fabricated filter I.

passband frequency can be tuned from 1.40 to 2.14 GHz with a 3-dB FBW of 11%.

The return loss is better than 12 dB in the overall tuning range of both passbands, as shown in Fig. 9(a). The insertion loss varies from 0.85 to 2.42 dB at the first passband frequency, whereas it varied 1.20 to 3.30 dB at the second passband frequencies, as shown in Fig. 9(b). As the passbands are tuned toward lower frequencies, the insertion loss becomes higher because the microstrip line becomes electrically shorter as a result, decreasing the overall resonator Q value.

For each bias voltage, the proposed filter provides three transmission zeros near the passbands in order to improve the selectivity of the filter. The two transmission zeros generated by two arms (from the tapping position to two ends of open loop, as shown in Fig. 7) corresponds to an electrical length of 90° at the frequencies of transmission zeros. The remaining transmission zero located on the higher side of the second passband is generated as result of the input impedance viewed from the tapping position toward center loaded varactor diode, and approaches zeros at the frequency of a transmission zero. These transmission zeros move along the passbands.

Fig. 10 shows the simulation and measurement results of filter I with the fixed first passband and controllable second passband frequency. As seen from this figure, the first passband frequency is constant at 1.070 GHz with 3-dB FBWs of 13% by keeping the bias voltage of varactor diodes connected at the line ends fixed. The second passband is controlled with the bias voltage of the varactor diode loaded at the center of the line. From the measurement result, it is found that the second passband frequency can be tuned from 1.70 to 1.98 GHz with almost constant 3-dB FBWs of 11%. The return loss is better than 15 dB for entire tuning range of the second passband, as shown in Fig. 10(a). The insertion loss varies from 1.15 to 2.76 dB, as shown in Fig. 10(b). Fig. 11 shows a photograph of the fabricated filter I.

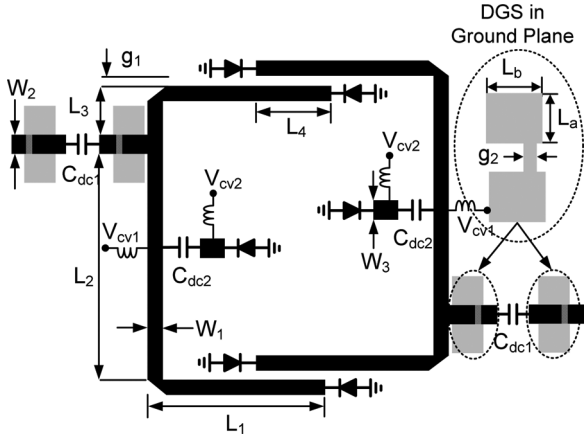

Fig. 12. Configuration of filter II and physical dimensions: $L_1 = 17.2$, $L_2 = 27.6$, $L_3 = 5.3$, $L_4 = 10$, $W_1 = 1.8$, $W_2 = 4.5$, $W_3 = 1.8$, $L_a = L_b = 6$, $g_1 = 0.64$, $g_2 = 0.4$, $C_{dc1} = 20$ pF, $C_{dc2} = 3.90$ pF. (Physical unit: millimeters).

B. Filter II: Tunable Dual-Band BPF With Harmonic Suppression

From the simulation and measurement results described in Section III-A, it is found that there are several harmonics of the two passbands and these harmonics are also tuned by varying the passband frequencies. These unwanted harmonics generated by the filter must be suppressed. A simple method of suppressing the harmonic is to introduce a transmission zero at the harmonic frequency [30]. However, this method will be inefficient because it can only suppress the harmonics around a specific frequency. In the case of the tunable dual-band BPF, the range of variation of the harmonic frequency variation is too broad, which are not sufficient to cancel harmonics by the simple transmission zero circuit.

The DGS of the microstrip line is implemented by making artificial defects on the ground plane and provides band-rejection characteristics at a certain resonance frequency band corresponding to the size of defect and its shape on the ground plane. The DGS also provides an additional effective inductance of the transmission line, which enables the slow-wave factor of line to be increased. These band-rejection properties and slow-wave effect of the DGS have been applied in the design of various microwave circuits such as filters, dividers, and amplifiers [31]–[33]. In microwave circuits, the band-rejection property of the DGS can also be utilized in the suppression of harmonics [34]–[37].

Fig. 12 shows the proposed configuration of the harmonic suppressed tunable dual-band filter II. In this structure, DGS is used at the input/output feeding lines for inducting coupling and acts as a broad band-rejection resonator to suppress the harmonics of filter I. The methods for finding the equivalent circuits of DGS are detailed in [33]. The EM simulation was performed using Ansoft's HFSS v11 while considering ideal capacitors. After simulation, the physical parameters and component values of the filter are determined as shown in Fig. 12.

Fig. 13 shows the simulation and measurement results of filter II. The passband frequencies are controlled with the help of the bias voltages of the varactor diodes. From the

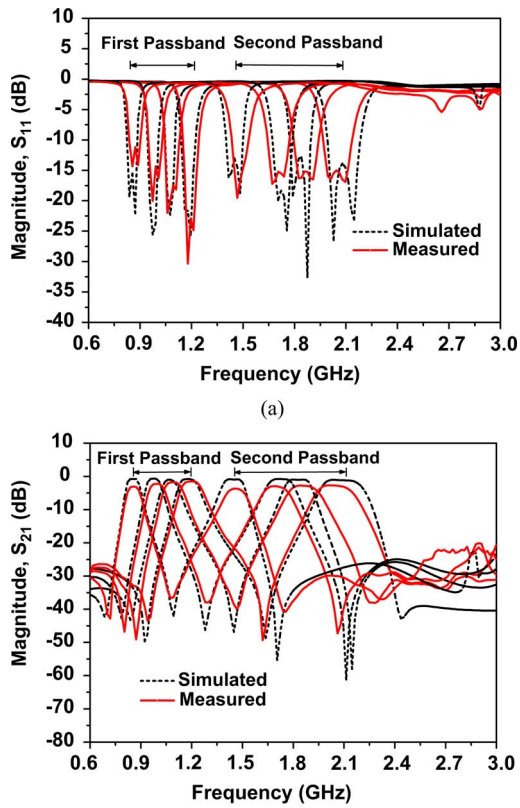

Fig. 13. Simulation and measurement results of filter II with tunable both passbands. (a) Return-loss and (b) insertion-loss characteristics. Reverse-bias voltage variation: $V_{Cv1} = 1.8 \sim 15$ V and $V_{Cv2} = 1 \sim 15$ V.

measurement results, the first passband frequency can be tuned from 0.85 to 1.2 GHz with 3-dB FBW of 13% and the second passband frequency can be tuned from 1.45 to 2.08 GHz with a 3-dB FBW of 11%. The return loss is better than 13 dB over the entire tuning range of the passbands, as shown in Fig. 13(a). The insertion loss varies from 1.32 to 3.4 dB at the first passband and 1.8 to 3.80 dB at the second passband, as shown in Fig. 13(b).

The differences in insertion loss between the simulation and measurement results are due to use of ideal capacitances in EM simulation. These measurement results for filter II are almost similar with filter I results provided in the previous section, except for the suppression of the harmonic characteristics.

Fig. 14 shows the simulation and measurement results of filter II with a fixed first passband and controllable second passband frequency. The first passband frequency is held constant at 1.070 GHz by fixing the bias voltage of varactor diodes connected to the ends of the line. The second passband frequency is tuned from 1.75 to 1.97 GHz. The return-loss variation is better than 15 dB throughout the tuning range of the passbands. Similarly, the variation of the insertion loss is 1.87 to 3.2 dB over the entire tuning range.

In order to verify the harmonic suppression characteristics of filter II, the broadband harmonic suppression characteristics are shown in Fig. 15. The stopband characteristics for fabricated filter II are better than -20 dB up to 18 GHz for the

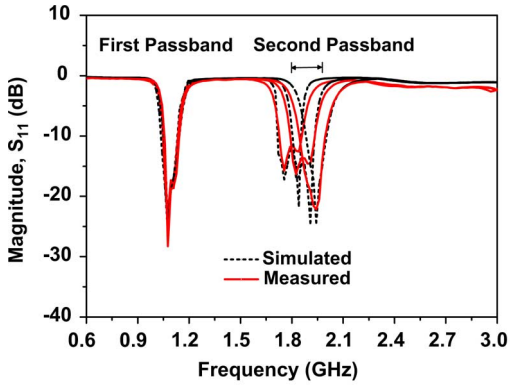

(a)

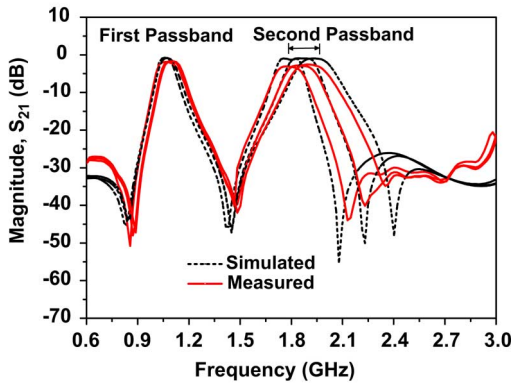

(b)

Fig. 14. Simulation and measurement result of filter II with fixed first passband and tunable second passband. (a) Return-loss and (b) insertion-loss characteristics. Reverse-bias voltage variation: $V_{Cv1} = 5.60$ V and $V_{Cv2} = 4.2 \sim 15$ V.

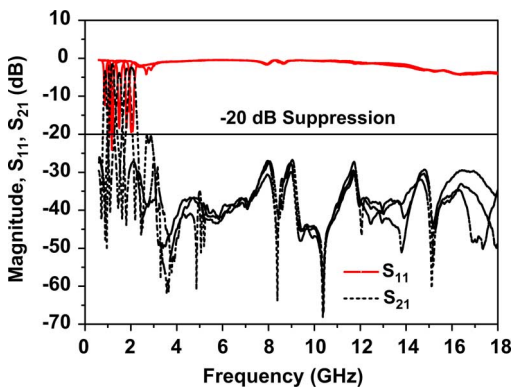

Fig. 15. Measured broadband harmonic suppression characteristics of filter II in overall tuning range passbands.

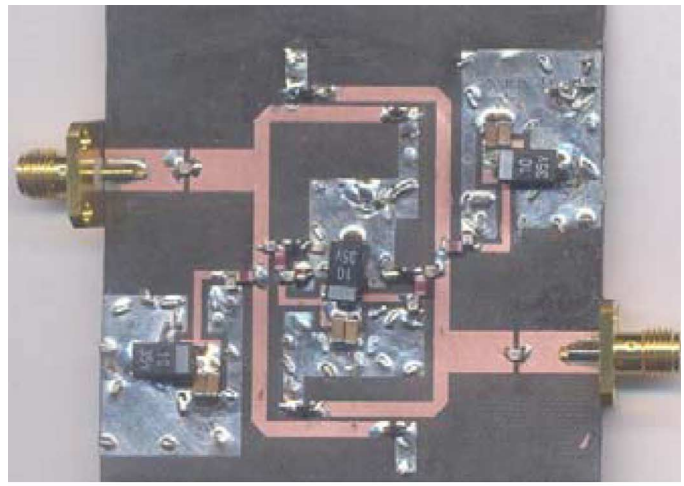

(a)

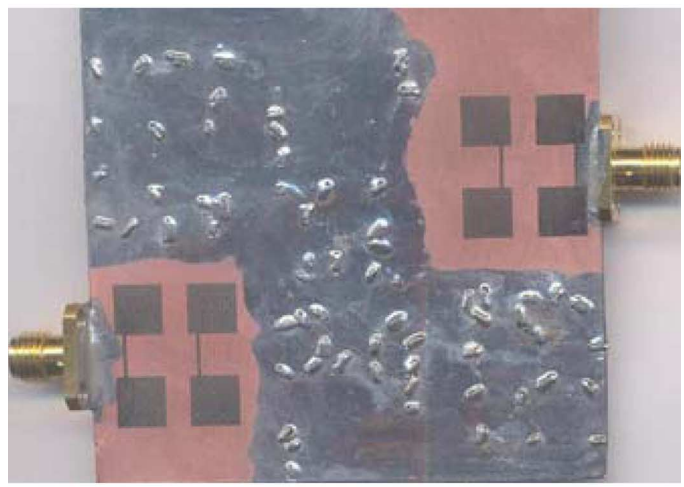

(b)

Fig. 16. Photograph of fabricated filter II. (a) Top side. (b) Bottom side.

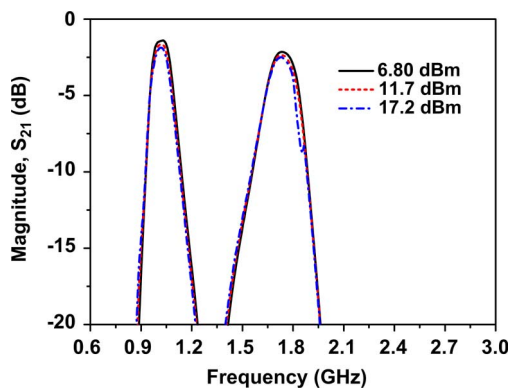

Fig. 17. Measured S_{21} with different input powers at bias voltages: $V_{cv1} = 3.7$ V and $V_{cv2} = 3.5$ V.

entire tuning range of the passbands. This means that the proposed structure can suppress more than tenth-order harmonics of the second passands due to band-rejection characteristics of DGS. This confirmed that the proposed method can achieve broadband harmonic suppression without degrading its passband's performances. Fig. 16 shows photographs of the fabricated filter II.

Fig. 17 presents the measured power handling capability of the proposed filter. From the measurement, it was found that the proposed filter can handle from 7- to 12-dBm power without any distortion in passbands. The input third-order intermodulation intercept point (IIP3) is measured around 1 and 2.14 GHz with 1-MHz spacing. The measured IIP3 is around 24 dBm and 29 dBm at 1 and 2.14 GHz, respectively.

Performance comparisons of the proposed tunable filter with other tunable filters reported in the literature are summarized in Table I. The proposed filter can provide the tunable dual-band passbands characteristics with broader frequency tunability

TABLE I
PERFORMANCE COMPARISON AMONG TUNABLE FILERS

	Frequency Tunablity [GHz]		Harmonic Suppression Order
	1st Passband	2nd Passband	
[10]	1.875-2.125	x	x
[12]	0.85-1.40	x	x
[13]	0.6-1.03	x	x
[15]	1.5-2.2	x	x
[16]	33.6-36/48.1-52.1	x	x
[17]	0.98-3.48*	x	x
[18]	Fixed @1.15	2.12-2.51	x
[19]	Fixed @2.43	5.28-5.74	x
[22]	2.20-2.7	3.45-4.20	-20dB up to $1.75f_2$
[25]	0.94-1.44	x	-15 dB up to $4f_1$
[26]	Fixed @ 2.40	Fixed @ 5.20	-22 dB up to $10f_1$
[27]	Fixed @ 2.45	Fixed @ 3.60	-20 dB up to $3f_1$
[28]	Fixed @ 2.40	Fixed @ 6.0	-30 dB up to $8.3f_1$
This work	**0.85-1.20**	**1.40-2.14**	**-20 dB more than to $10f_2$**

*Substrate Integrated evanescent-mode high Q-cavity filter

than previously proposed filters. The simultaneous dual-band frequency tuning and the only second band frequency tuning are also obtainable in addition to broadband harmonic rejection characteristics.

IV. CONCLUSION

In this paper, designs for harmonic suppressed tunable dual-band BPFs have been demonstrated. Both the theoretical analysis and experiments are described to validate the proposed structure. The DGSs are utilized to reject harmonics. The experimental results are in good agreement with the theoretical predictions. The experimental results showed that the first passband can be tuned within 34.1% frequency tunability range from 0.85 to 1.2 GHz and the second passband within 41.8% frequency tunability from 1.40 to 2.14 GHz with the constant fractional bandwidth and passband shape. The proposed method can suppress more than tenth-order harmonics of second passbands, thereby ensuring broadband rejection characteristics without any degradation of passband characteristics. For all the tuning states, transmission zeros are realized near the passband frequencies, which provides the high selectivity of the filter. The proposed filter design method can be applicable to selectable multimode or multiband applications.

REFERENCES

[1] K. Entesari and G. M. Rebeiz, "A differential 4-bit 6.5–10 GHz RF MEMS tunable filter," *IEEE Trans. Microw. Theory Tech.*, vol. 53, no. 3, pp. 1103–1110, Mar. 2005.

[2] S. Park, M. A. El-Tanani, I. Reines, and G. M. Rebez, "Low-loss 4–6 GHz tunable filter with 3-bit high Q-orthogonal bias RF-MEMS capacitance network," *IEEE Trans. Microw. Theory Tech.*, vol. 56, no. 10, pp. 2348–2355, Oct. 2008.

[3] A. Pothier, J. C. Orlianges, G. Zheng, C. Champeaux, A. Catherinot, P. B. D. Cros, and J. Papaplymerou, "Low-loss 2-bit tunable bandpass filters using MEMS DC contact switches," *IEEE Trans. Microw. Theory Tech.*, vol. 53, no. 1, pp. 354–360, Jan. 2005.

[4] K. Entersari and G. M. Rebeiz, "A 12–18 GHz three-pole RF MEMS tunable filter," *IEEE Trans. Microw. Theory Tech.*, vol. 53, no. 8, pp. 2566–2571, Aug. 2005.

[5] J. Nath, D. Ghosh, J. P. Maria, A. I. Kingon, W. Fathelbab, P. D. Franzon, and M. B. Steer, "An electronically tunable microstrip bandpass filter using thin-film barium–strontium–titante (BST) varactors," *IEEE Trans. Microw. Theory Tech.*, vol. 53, no. 9, pp. 2707–2712, Sep. 2005.

[6] I. Vendik, O. Vendik, V. Pleskachev, A. Svishchev, and R. Wordenweber, "Design of tunable ferroelectric filters with a constant fractional bandwidth," in *IEEE MTT-S Int. Microw. Symp. Dig.*, 2001, pp. 1461–1464.

[7] L. H. Hsieh and K. Chang, "Tunable microstrip bandpass filters with two transmission zeros," *IEEE Trans. Microw. Theory Tech.*, vol. 51, no. 2, pp. 520–525, Feb. 2003.

[8] B. Liu, F. Wei, and X. Shi, "Reconfigurable bandpass filter based on net-type stepped impedance resonator," *Electron. Lett.*, vol. 46, no. 22, pp. 1506–1507, Feb. 2010.

[9] I. C. Hunter and J. D. Rhodes, "Electronically tunable microwave band pass filters," *IEEE Trans. Microw. Theory Tech.*, vol. MTT-30, no. 9, pp. 1354–1360, Sep. 1982.

[10] B. W. Kim and S. W. Yun, "Varactor tuned combline bandpass filter using step-impedance microstrip lines," *IEEE Trans. Microw. Theory Tech.*, vol. 52, no. 4, pp. 1279–1283, Apr. 2004.

[11] A. R. Brown and G. M. Rebeiz, "A varactor tuned RF filter," *IEEE Trans. Microw. Theory Tech.*, vol. 48, no. 7, pp. 1157–1160, Jul. 2000.

[12] S. J. Park and G. M. Rebeiz, "Low loss two pole tunable filters with three different predefined bandwidth characteristics," *IEEE Trans. Microw. Theory Tech.*, vol. 56, no. 5, pp. 1137–1148, May 2008.

[13] W. Tang and J. Hong, "Varactor-tuned dual-mode bandpass fitlers," *IEEE Trans. Microw. Theory Tech.*, vol. 58, no. 8, pp. 2213–2219, Aug. 2010.

[14] J. Long, C. Li, W. Cui, J. Huangfu, and L. Ran, "A tunable microstrip bandpass filter with two independently adjustable transmission zeros," *IEEE Microw. Wireless Compon. Lett.*, vol. 21, no. 2, pp. 74–76, Feb. 2011.

[15] Y. Chiou and G. M. Rebeiz, "A tunable three-pole 1.5–2.2 GHz bandpass filter with bandwidth and transmission zero control," *IEEE Trans. Microw. Theory Tech.*, vol. 59, no. 11, pp. 2872–2878, Nov. 2011.

[16] H. Jiang, B. Lacroxi, K. Choi, Y. Wang, A. T. Hunt, and J. Papapolymerou, "Ka- and U-band tunable bandpass filters using ferroelectric capacitors," *IEEE Trans. Microw. Theory Tech.*, vol. 59, no. 12, pp. 3068–3074, Dec. 2011.

[17] S. Moon, H. H. Sigmarsson, H. Joshi, and W. J. Chappell, "Substrate integrated evanescent-mode cavity filter with a 3.5 to 1 tuning ratio," *IEEE Microw. Wireless Compon. Lett.*, vol. 20, no. 8, pp. 450–452, Aug. 2010.

[18] X. Y. Zhang and Q. Xue, "Novel centrally loaded resonators and their applications to bandpass filters," *IEEE Trans. Microw. Theory Tech.*, vol. 56, no. 4, pp. 913–921, Apr. 2008.

[19] D. Girbau, A. Lazaro, E. Martinez, D. Masone, and L. Pradell, "Tunable dual-band bandpass filter for WLAN applications," *Microw. Opt. Technol. Lett.*, vol. 51, no. 9, pp. 2025–2028, Sep. 2009.

[20] D. Girbau, A. Lazaro, A. Parez, E. Martinez, L. Pradell, and R. Villarino, "Tunable dual-band filters based on capacitive loaded stepped impedance resonators," in *Proc. 39th Eur. Microw. Conf.*, 2009, pp. 113–116.

[21] G. Chaudhary, H. Choi, Y. Jeong, J. Lim, D. Kim, and J.-C. Kim, "Design of dual-band bandpass filter using DGS with controllable second passband," *IEEE Microw. Wireless Compon. Lett.*, vol. 21, no. 11, pp. 589–891, Nov. 2011.

[22] E. E. Djoumessi, M. Chaker, and K. Wu, "Varactor-tuned quarter-wavelength dual-bandpass filter," *IET Microw. Antenna, Propag.*, vol. 3, no. 1, pp. 117–124, Feb. 2009.

[23] H. J. Park, J. Y. Park, J. C. Lee, J. H. Kim, B. Lee, N. Y. Kim, and U. S. Hong, "A new varator tuned microstrip ring bandpass filter with harmonic suppression," in *Proc. Asia–Pacific Microw. Conf.*, 2000, pp. 1127–1130.

[24] X. Y. Zhang, Q. Xue, C. H. Chan, and B. J. Hu, "Low-loss frequency agile bandpass filters with controllable bandwidth and suppressed second harmonic," *IEEE Trans. Microw. Theory Tech.*, vol. 58, no. 6, pp. 1557–1564, Jun. 2010.
[25] X. Y. Zhang and Q. Xue, "High selectivity tunable bandpass filters with harmonic suppression," *IEEE Trans. Microw. Theory Tech.*, vol. 58, no. 4, pp. 964–969, Apr. 2010.
[26] M. Jiang, H. P. Lin, and J. T. Kuo, "Design of quasi-elliptic function filters with dual-passband responses with multi-spurious suppression," in *Proc. Asia–Pacific Microw. Conf.*, 2007, pp. 2365–2368.
[27] M. Mokhtaari, K. Rambabu, J. Bornemann, and S. Amari, "Advanced stepped-impedance dual-band filters with wide second stopbands," in *Proc. Asia–Pacific Microw. Conf.*, 2007, pp. 2285–2288.
[28] J. T. Kuo and H. P. Lin, "Dual-band bandpass filter with improved performances in extended upper rejection band," *IEEE Trans. Microw. Theory Tech.*, vol. 57, no. 4, pp. 824–829, Apr. 2009.
[29] J. Hong and M. J. Lancaster, *Microstrip fitlers for RF/Microwave Applications*. New York: Wiley, 2001.
[30] S. Sun and L. Zhu, "Periodically non-uniform coupled microstrip-line filter with harmonic suppression using transmission zero reallocation," *IEEE Trans. Microw. Theory Tech.*, vol. 53, no. 5, pp. 1817–1822, May 2005.
[31] D. Ahn, J. S. Park, C. S. Kim, J. N. Kim, Y. Qian, and T. Itoh, "A design of low-pass filter using the novel microstrip defected ground structure," *IEEE Trans. Microw. Theory Tech.*, vol. 49, no. 1, pp. 86–93, Jan. 2001.
[32] J. S. Lim, S. W. Lee, C. S. Kim, J. S. Park, D. Ahn, and S. Nam, "A 4:1 unequal Wilkinson power divider," *IEEE Microw. Wireless Compon. Lett.*, vol. 11, no. 3, pp. 124–126, Mar. 2001.
[33] Y. Jeong, S. Jeong, J. Lim, and S. Nam, "A new method to suppress harmonics using $\lambda/4$ bias line combined by defected ground structure in power amplifier," *IEEE Microw. Wireless Compon. Lett.*, vol. 13, no. 12, pp. 538–540, Dec. 2001.
[34] J. Park, J. Kim, and S. Nam, "Design of a novel harmonic suppressed microstrip low-pass filter," *IEEE Microw. Wireless Compon. Lett.*, vol. 17, no. 6, pp. 424–426, Jun. 2007.
[35] D. Woo and T. Lee, "Suppression of harmonics in Wilkinson power divider using dual-band rejection by asymmetric DGS," *IEEE Trans. Microw. Theory Tech.*, vol. 53, no. 6, pp. 2139–2144, Jun. 2005.
[36] C. Kim, D. Kim, I. Song, K. Leong, T. Itoh, and D. Ahn, "A design of a ring bandpass filters with wide rejection band using DGS and spur-line coupling structures," in *IEEE MTT-S Int. Microw. Symp. Dig.*, 2005, pp. 2183–2186.
[37] J. Lim, C. Kim, D. Ahn, Y. Jeong, and S. Nam, "Design of low-pass filters using defected ground structure," *IEEE Trans. Microw. Theory Tech.*, vol. 53, no. 8, pp. 2539–2545, Aug. 2005.

Girdhari Chaudhary (S'10) received the B.E. degree in electronics and communication engineering from the Nepal Engineering College (NEC), Kathmandu, Nepal, in 2004, the M.Tech degree in electronics and communication engineering from the Malaviya National Institute of Technology (MNIT), Jaipur, India, in 2007, and is currently working toward the Ph.D. degree at Chonbuk National University, Jeonju, Korea.

His research interests include multiband passive circuits, negative group-delay filters, and high-efficiency power amplifiers.

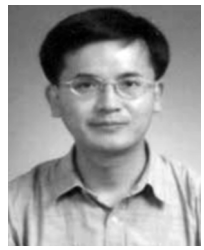

Yongchae Jeong (M'99–SM'10) received the BSEE, MSEE, and Ph.D. degrees in electronics engineering from Sogang University, Seoul, Korea, in 1989, 1991, and 1996, respectively.

From 1991 to 1998, he was a Senior Engineer with Samsung Electronics. Since 1998, he has been with the Division of Electronic Engineering, Chonbuk National University, Jeonju, Korea. From July 2006 to December 2007, he was with the Georgia Institute of Technology, as a Visiting Professor. He is currently a Professor and Associate Dean of the College of Engineering, and a member of the Information Technolgoy Convergence Research Center, Chonbuk National Univeristy. He currently teaches and conducts research in the area of microwave devices, base-station amplifiers, nonlinear devices, system linearizing technology, and RF integrated circuit (RFIC) design. He has authored and coauthored over 100 papers in international journals and conference proceedings.

Dr. Jeong is a member of the Korea Institute of Electromagnetic Engineering and Science (KIEES).

Jongsik Lim (S'90–M'93–SM'05) received the B.S. and M.S. degrees in electronic engineering from Sogang University, Seoul, Korea, in 1991 and 1993, respectively, and the Ph.D. degree from the School of Electrical Engineering and Computer Science, Seoul National University, Seoul, Korea, in 2003.

In 1993, he joined ETRI, Daejeon, Korea, where he remained for six years as part of the Satellite Communication Division as a Senior Member of Research Staff as was one of the key members who developed monolithic microwave integrated circuit (MMIC) low-noise amplifiers (LNAs) and solid-state power amplifiers (SSPAs) for 20/30-GHz satellite transponders. From March to July 2003, he was with the Division of Information Technology, Seoul National University (under the Brain Korea 21 Project), a Post-Doctoral Fellow, during which time he gave lectures at the graduate schools of Soonchunhyang University and Soongsil University. From July 2003 to September 2004, he was a Patent Examiner with the Korean Intellectual Property Office (KIPO). In September 2004, he rejoined ETRI as a Senior Research Member with the Antenna Technology Research Team/Radio Technology Group. Since March 2005, he has been with the Department of Electrical and Communication Engineering, Soonchunhyang University, Chungcheongnam-do, Korea, as a faculty member. His current research interests include design of the passive and active circuits for RF/microwave and millimeter-wave with microwave integrated circuit (MIC)/MMIC technology, modeling of active device, design of high-power amplifiers for mobile communications, applications of periodic structure to RF/microwave circuits, and modeling of passive structure having periodic structures.

Dr. Lim is a member of the Institute of Electronics, Information and Communication Engineers (IEICE), Japan, and the Korea Institute of Electromagnetic Engineering and Science (KIEES).